

K.D. Lawson, J. Zacks, I.H. Coffey  
and JET EFDA contributors

# A Relative Sensitivity Calibration of the JET KT7/2 Spectrometer

"© – COPYRIGHT ECSC/EEC/EURATOM, LUXEMBOURG – 2009"

"Enquiries about Copyright and reproduction should be addressed to the  
Publications Officer, EFDA, Culham Science Centre, Abingdon, Oxon, OX14 3DB, UK."

# A Relative Sensitivity Calibration of the JET KT7/2 Spectrometer

K.D. Lawson<sup>1</sup>, J. Zacks<sup>1</sup>, I.H. Coffey<sup>2</sup>  
and JET EFDA contributors\*

<sup>1</sup>*EURATOM/UKAEA Fusion Association, Culham Science Centre, OX14 3DB, UK.*

<sup>2</sup>*Astrophysics Research Centre, School of Mathematics and Physics, Queen's University, Belfast,  
BT7 1NN, Northern Ireland, UK*

*\*See annex of F. Romanelli et al, "Overview of JET Results",  
(Proc. 22 nd IAEA Fusion Energy Conference, Geneva, Switzerland (2008)).*



# A relative sensitivity calibration of the JET KT7/2 spectrometer

K D Lawson<sup>1</sup>, J Zacks<sup>1</sup> & I H Coffey<sup>2</sup> & JET-EFDA Contributors\*

*JET-EFDA, Culham Science Centre, Abingdon, OX14 3DB, UK*

<sup>1</sup> *Euratom/UKAEA Fusion Association, Culham Science Centre, Abingdon, OX14 3DB, UK*

<sup>2</sup> *Astrophysics Research Centre, School of Mathematics and Physics, Queen's University, Belfast, BT7 1NN, Northern Ireland, UK*

## Abstract

As a first step in determining a full absolute sensitivity calibration for the present KT7 spectrometers a relative calibration for the KT7/2 spectrometer is presented. This has been achieved using a novel approach, which proved particularly successful in the short wavelength calibration of the KT2 spectrometer (Lawson *et al.*, 2009a). The measured and modelled line intensity ratios of a number of Na- and Li-like metal doublets are compared allowing their relative sensitivities to be found at the doublet wavelengths. Where pairs of wavelengths overlap, the calibration can be extended to shorter or longer wavelengths. As with the KT2 calibration, this procedure has resulted in a particularly accurate calibration, which in the present case extends throughout most of the spectrometer's wavelength range. In addition, it has been possible to use comparisons of measured and modelled CIV line intensity ratios to provide a check on the derived calibration and to allow the calibration at the longest wavelengths to be improved. The KT7 line profiles are such that weak spectral lines require a narrower integration range than is used for intense lines and the ratio of the integrations made with the full and narrow ranges is derived allowing the calibration to be used to give reliable measurements of weak spectral lines.

## 1. Introduction

In order to make full use of the data recorded with the KT7 spectrometer (Wolf *et al.*, 1995) it is necessary to determine the instrument's sensitivity calibration. Of immediate interest is the analysis of the C spectrum, since discrepancies have been found between the observed C emission from the Scrape-Off-Layer (SOL) of the JET plasma and modelled line intensity ratios (Lawson *et al.*, 2009b and Zacks, 2009). The KT7 detector that observes the 140Å to 443Å spectral range, KT7/2, is ideal for this study, since it covers the emission from the CIV ionization stage. This stage is the one that has been most extensively investigated. It is found that, in contrast to the SOL emission, a consistent analysis is possible for the CIV radiation from the JET divertor.

The calibration is derived from the comparison of modelled and measured line intensity ratios of a number of Na- and Li-like doublets of metallic elements and the noble gas Ar, as was done for the short wavelength end of the KT2 sensitivity calibration (Lawson *et al.*, 2009a). Such lines fall throughout the detector's spectral range and are ideal for deriving a sensitivity calibration, since the doublet line intensity ratios are independent of electron density and almost insensitive to the electron temperature. The line intensity ratio can therefore be modelled with minimal uncertainty. It was also possible to use the CIV emission from the divertor to confirm the derived calibration and to improve the calibration at the longest wavelengths.

This work continues and extends the work of Maggi (1996) and Zacks (2009), who present sensitivity calibrations for the original detectors used in the spectrometer. The calibration given here is for the present detector, the original microchannel plate (MCP) being replaced in 1998.

Section 2 gives a brief description of the spectrometer and section 3 discusses the modelling of the doublet line intensity ratios, the measurements and the derivation of the relative calibration. The application of the calibration to weak spectral lines is also discussed in this section. Conclusions are presented in section 4.

## 2. Experimental arrangement

The KT7 diagnostic consists of three spectrometers, two SPRED instruments (KT7/1 and KT7/2) (Fonck *et al.* 1982) and a Schwob-Fraenkel SOXMOS instrument (KT7/3) (Schwob *et al.*, 1987). The latter, in contrast to the KT4 spectrometer, only has a single detector. The instrument has a vertical line of sight looking from the top of the machine into the JET divertor. The diagnostic can be tilted poloidally allowing the line of sight to view anywhere from the inner divertor through to the SOL above the throat of the outer divertor. The Na- and Li-like data used to obtain the calibration were recorded with this outermost line of sight, the C data with a view into the divertor plasma. The SPREDS are enclosed in stainless steel shielding to reduce noise due to both neutrons and  $\gamma$ -rays, there being 15cm of shielding between the plasma and detectors and 5cm thickness at the back and sides. The detectors consist of MCP / phosphor combinations which are coupled to a Reticon photodiode via a fibre optic bundle. It is the interaction of the neutrons and  $\gamma$ -rays with the MCP, with its high gain, that is of most concern. A shielding of 15cm of steel was expected to reduce the neutron flux by a factor of  $\sim 8$  and that of 8MeV  $\gamma$ -rays by a factor of  $\sim 17$ . Comparisons between KT2 and KT7 shortly after the latter was first commissioned suggested that the background due to nuclear reaction products was a factor  $\sim 7$  lower in KT7 than the unshielded KT2.

Originally, 0.5mm thick MCPs were installed in the SPREDS, but were found to be very fragile. In 1998 they were replaced with 1mm thick MCPs, which also gave increased sensitivity. The derived KT7/2 calibration is for the present detector. The MCPs have a CuI coating. Both KT7/1 and KT7/2 use toroidal holographic gratings, the former with a ruling density of  $450 \text{ g.mm}^{-1}$ , KT7/2 with  $2105 \text{ g.mm}^{-1}$ . Both have extended and shifted spectral ranges compared to the standard SPREDS. KT7/2 observes a range  $140\text{\AA}$  to  $443\text{\AA}$  with a spectral resolution of  $\sim 1\text{\AA}$ . Normally the gratings enhance the first and third spectral orders, but in the case of KT7/2 the second spectral order is seen weakly, but with a greater intensity than the third.

Both SPREDS have 2048 pixels, although the KT7/2 detector developed a fault in which adjacent pairs of pixels output the same reading, essentially reducing the useful number of pixels to 1024. A simple and reliable line integration method was employed, in which a particular number of pixels on either side of the line centre define an integration range and a background to be subtracted. This method takes advantage of the similarity of the spectral line profile throughout the spectral range of the instrument. The integration is performed using Simpson's rule. With 2048 pixels a  $\pm 5$  pixel integration range is preferred. However, with only 1024 pixels a  $\pm 3$  pixel range is ideal for intense lines, but is too wide for weak lines. For intense lines the  $\pm 3$  pixel range covers almost the full line profile, whereas a  $\pm 2$  pixel range is thought too narrow to ensure a reliable integration. In weak lines, the third pixel on either side of the line centre tends to be absorbed into the background and therefore will not be reliable; consequently, a  $\pm 2$  pixel range is the maximum that can be used. The calibration is derived using intense lines for which the  $\pm 3$  pixel range is used. In order to measure weak lines the ratio of the  $\pm 3$  to  $\pm 2$  pixel integrations is also required.

The design of the diagnostic is particularly robust making the spectrometer very stable mechanically. This is advantageous in running the instrument on JET with its long period of operations during which there is limited access to the machine.

### 3. Derivation of the sensitivity calibration

#### a) Na- and Li-like doublets

The Na- and Li-like doublets of a number of intrinsic metallic impurities are observed throughout the KT7/2 spectral range. They correspond to the  $2p^63s\ ^2S_{1/2} - 2p^63p\ ^2P_{1/2,3/2}$  and  $1s^22s\ ^2S_{1/2} - 1s^22p\ ^2P_{1/2,3/2}$  transitions, respectively. In addition, the noble gases Ar and Kr can be introduced into the plasma by gas puffing, these elements having a similar doublet structure. Figure 1 shows the KT7/2 spectrum for pulse 67966 averaged between times 9.3 and 9.4s. Doublets belonging to Cr, Fe, Ni and Cu can be seen. In addition one of the MnXXIII lines and the ArXVI and CrXIV doublets appear weakly in this spectrum. In contrast, the 192.0Å line of the FeXXIV doublet is saturated and the 132.9Å FeXXIII line, which is expected to be of a similar intensity, can be seen weakly in the second and third orders. A comparison of the modelled and measured doublet line intensity ratios gives the ratio of sensitivities at the doublet wavelengths. Neighbouring doublets can then be used to extend the calibration to either shorter or longer wavelengths.

Table 1. Na-like doublet modelled line intensity ratios

Ion	Wavelengths (Å)	Ionization potential (eV)	Modelled intensity ratio	Source
CrXIV	389.9 / 412.0	384	1.96	Intrinsic
FeXVI	335.4 / 360.8	489	1.95	Intrinsic
NiXVIII	292.0 / 320.6	607	1.94	Intrinsic
KrXXVI	179.0 / 220.0	1205	1.88	Gas puffed

These intensity ratios are ideal for determining the sensitivity calibration, since they are found to be insensitive to  $n_e$  and are only very weakly dependent on  $T_e$ . They are modelled using the collisional-radiative model, in which the energy level populations are determined from electron collisional excitation and de-excitation and radiative decay. Ratios were calculated at the temperature corresponding to the ionization potential and at half and double this temperature. Since the ratios differed by less than 2% over this wide temperature range, the values for the central temperatures were adopted. Sampson *et al.* (1990) and Zhang *et al.* (1990) have provided relativistic distorted wave calculations for the electron collisional excitation rates for, respectively, the Na- and Li-like ionization stages for a wide range of elements and there are R-matrix calculations for ArXVI and FeXXIV by Whiteford *et al.* (2002). Comparisons of the line intensity ratios modelled using the different electron rates, calculated with the ADAS atomic data package (Summers, 2004), show agreement to within ~1%. Interpolated values were obtained for those elements for which there are no published data and an adjustment was made to account for the marginally higher (~1%) ArXVI and FeXXIV R-matrix values. It is expected that the derived line intensity ratios are accurate to a few per cent.

Table 2. Li-like doublet modelled line intensity ratios

Ion	Wavelengths (Å)	Ionization potential (eV)	Modelled intensity ratio	Source
ArXVI	353.9 / 389.1	918	1.97	Gas puffed
CrXXII	223.0 / 279.7	1722	1.93	Intrinsic
MnXXIII	206.9 / 266.9	1880	1.92	Intrinsic
FeXXIV	192.0 / 255.1	2046	1.91	Intrinsic
NiXXVI	165.4 / 234.2	2399	1.88	Intrinsic
CuXXVII	153.5 / 224.7	2585	1.87	Intrinsic

In all, measurements of ten doublet ratios were made. Their wavelengths, ionization potentials and the modelled intensity ratios are listed in tables 1 and 2. It can be seen that they cover wavelengths from 153.5Å up to 412.0Å, almost the complete range of the KT7/2 detector. Most of the wavelength intervals overlap. In these cases, the calibration was extended by making a linear interpolation of the logarithm of the inverse sensitivity to the intermediate wavelength of the overlapping doublet. The sensitivity at the other wavelength of this doublet can then be found. There are three gaps in the wavelength coverage, 279.7Å to 292.0Å, 320.6Å to 335.4Å and a small jump from 389.1Å to 389.9Å. To bridge the gaps, the gradient of the logarithm of the inverse sensitivity of the interval was taken to be the mean of those on either side.

Table 3. Comparison of Na-like doublet line intensity ratios

Ion	Modelled intensity ratio	Measured intensity ratio	Inverse sensitivity ratio	Number of pulses	Reliability
CrXIV	1.96	2.64 $\pm$ 3.3%	0.743	12	C
FeXVI	1.95	2.34 $\pm$ 2.8%	0.833	12	B
NiXVIII	1.94	2.29 $\pm$ 2.1%	0.849	21	A
KrXXVI	1.88	2.72 $\pm$ 1.5%	0.690	12	B

A indicates most reliable, D least reliable

Tables 3 and 4 give comparisons for the Na- and Li-like doublet lines, respectively, of the modelled and measured line intensity ratios, together with the derived inverse sensitivity ratios, the number of pulses averaged in obtaining a measurement and estimates of their reliability. Figure 2 illustrates this by showing the wavelength extent and inverse sensitivity ratios of the doublets. As was found in the analysis of the short wavelength section of the KT2 spectrum (Lawson *et al.* 2009a) line blending is still a significant problem, despite the spectral resolution of KT7/2 being a factor of  $\sim$ 5 better than that of KT2. This is because the search for Na- and Li-like lines concentrated on the period when KT7/2 was viewing the SOL above the throat of the outer divertor. With this view the spectrum is much less affected by the low  $Z$  emission that dominates the spectrum when the line of sight is towards the divertor box. There were about half the number of pulses during this period, pulses 65988 to 69890, than were searched in the KT2 analysis,  $\sim$ 3900 rather than  $\sim$ 7400, and the spectra were less rich in intense metal lines at this time. For example, only 4 CrXXII measurements out of the 21 made and 5 NiXXVI measurements out of 31 were intense, free from blends and neighbouring lines and with a good match between the time histories of the two doublet components. Despite this, various means of the full and partial datasets only differed from the mean of the most reliable pulses by a few per cent. In the case of CrXXII, even the most extreme means were within  $\pm$ 8% of the preferred value and for NiXXVI the means fell within the range -5% to +1% of the preferred mean. It follows that the final value of the measured ratio taken is not particularly sensitive to the choice of the pulses used, this giving confidence in the derived calibration.

Table 4. Comparison of Li-like doublet line intensity ratios

Ion	Modelled intensity ratio	Measured intensity ratio	Inverse sensitivity ratio	Number of pulses	Reliability
ArXVI	1.97	2.36 $\pm$ 2.2%	0.836	11	B
CrXXII	1.93	2.80 $\pm$ 1.9%	0.689	4	C
MnXXIII	1.92	3.27	0.588	1	D
FeXXIV	1.91	3.49 $\pm$ 2.9%	0.548	9	C
NiXXVI	1.88	2.59 $\pm$ 2.5%	0.726	5	C
CuXXVII	1.87	2.41 $\pm$ 3.6%	0.775	20	C

A indicates most reliable, D least reliable



The FeXXIV and CuXXVII doublet ratios are even more extreme. In the case of FeXXIV, the doublet lines are particularly prone to blending and only one pulse, 66410, is expected to give a reliable result. At the time the measurements were made, low levels of He were present in the plasma, these being sufficient for the 256.3Å HeII line to affect nearly all of the FeXXIV 255.1Å measurements. In all the pulses studied for the CuXXVII doublet ratio, the CrXXII line at 223.0Å, to a lesser or greater extent, affects the integration of the 224.7Å line, the weaker member of the CuXXVII doublet.

It was therefore necessary to carry out line profile fits for both the FeXXIV and CuXXVII ratios. In the case of FeXXIV, double Gaussian fits were made to both Fe lines in order to account for the 193Å OV multiplet and the 256.3Å HeII line, which appeared to be the most troublesome blends. For CuXXVII, allowance was made for the CrXXII line at 223.0Å again using a double Gaussian fit. Only the line centre approximates to a Gaussian shape and the limitations of using this profile were evident particularly in this last case. Consequently, different fits were tried for CuXXVII to ensure that this approximation did not introduce significant errors. For the majority of the cases considered, the results are expected to be accurate to a few per cent. It is also noted that with line fitting, the FeXXIV and CuXXVII measured ratios only changed by 11% and -6%, respectively, from the measurements without line fits. That for Fe, in particular, is expected to be a significant improvement.

Mn is only rarely seen in JET and of the four pulses in which measurements were made only one was considered reliable. With only one measurement this ratio must be regarded as being of limited reliability.

The CrXIV doublet falls at the least sensitive end of the detector and even then is never seen as intensely as the other Na- and Li-like doublets. For this line ratio, it is necessary to be aware of a blend of the 389.9Å line with the ArXVI line at 389.1Å. In the analysis, the ArXVI 353.9Å line was used to monitor the Ar level. There is confidence in the derived ratio in that the means of the full database of 36 measurements and various partial datasets differed by no more than 1.1% from the preferred mean, although the modest intensity of the lines make these measurements of more limited reliability than for some of the other ratios.

In contrast to the analysis for the KT2 calibration in which the KrXXVI doublet ratio did not fit the trend of the other data, in the present case, the KrXXVI measurement is found to be consistent with the other measurements.

## b) CIV line intensity ratios.

Despite the above comments and caveats, it can be seen that the magnitude of the differences and errors being discussed is small compared with the accuracy of many VUV calibrations, being closer to that expected for visible systems. Consequently, a very satisfactory calibration for the KT7/2 spectrometer is expected and, indeed, between 223Å and 361Å the calibration closely follows a straight line in logarithmic space. Above this wavelength, the calibration unexpectedly deviates from the straight line. This is a result of the ArXVI measurement, which is expected to be reliable. Although the difference of the derived calibration from the straight line is only small, 7%, it has to be remembered that a step by step procedure is being used to derive the calibration. Therefore to ensure that there is no cumulative error being introduced, it is thought advisable to use an independent check..

This can be done using the CIV line intensities emitted from the divertor plasma. Again modelled and measured line intensity ratios are compared, although in this case the model is more complicated, since the CIV ratios depend on the electron temperature and density and recombination, particularly charge exchange recombination, must be considered as a populating mechanism. Six CIV lines, shown in spectrum in figure 3 and listed in table 5, have been used in the analysis. A check was made as to the effect of the CIII line at 386.2Å on the integration of the 384.1Å line and this was found to be at most 2%. It is also noted that the three lowest

wavelength lines were comparatively weak, a  $\pm 2$  pixel integration range being used in their integration. Ratios were measured during the ohmic phase in 86 pulses and the additionally heated phase in 165 pulses. The line intensity is given by

$$I = n_e n_g \epsilon^{exc} + n_e n_{g+1} \epsilon^{rec} + n_D n_{g+1} \epsilon^{cx},$$

where  $n_e$  and  $n_D$  are the electron and deuteron densities,  $n_g$  and  $n_{g+1}$  the ground state densities of the CIV and CV ionisation stages, respectively, and  $\epsilon$  the Photon Emissivity Coefficients (PECs) as used in ADAS. The PECs give the contribution to the line intensity of electron excitation and recombination, the latter being separated into charge exchange recombination and other recombination processes, including dielectronic, radiative and three body recombination. The electron excitation rates were derived from the R-matrix calculations of Aggarwal and Keenan (2004), the other atomic data being taken from the ADAS database.

Table 5. CIV lines used in analysis.

Wavelength (Å)	Transition	Comment
244.9	$1s^2 2s^2 S_{1/2} - 1s^2 4p^2 P_{1/2,3/2}$	Weak intensity
289.2	$1s^2 2p^2 P_{1/2,3/2} - 1s^2 4d^2 D_{3/2,5/2}$	Weak intensity
296.9	$1s^2 2p^2 P_{1/2,3/2} - 1s^2 4s^2 S_{1/2}$	Weak intensity
312.4	$1s^2 2s^2 S_{1/2} - 1s^2 3p^2 P_{1/2,3/2}$	
384.1	$1s^2 2p^2 P_{1/2,3/2} - 1s^2 3d^2 D_{3/2,5/2}$	Blend - CIII, 386.2Å
419.6	$1s^2 2p^2 P_{1/2,3/2} - 1s^2 3s^2 S_{1/2}$	

Line intensity ratios were calculated relative to the 312.4Å line and the discrepancies between the modelled and measured ratios found. In this analysis, the minimum rms difference between the modelled and measured ratios was determined for each measurement and then the resulting differences averaged for each line ratio. These were less than 9%, apart from that for the 384.1Å / 312.4Å ratio, which was 16.5%. They were taken to be the discrepancy in the calibration. A second order polynomial fit was then made to both the CIV and the Na- and Li-like calibration points. Since the measured CIV ratios themselves depend on the sensitivity calibration, two iterations were required before subsequent changes in the calibration were less than 1%. Further information regarding the procedure used is given by Lawson *et al.* (2009c).

The relative sensitivity calibration and final polynomial fit is shown in figure 4, the coefficients of the polynomial being given in table 6. The sensitivity at 312.4Å is taken to be 1. It can be seen that the three shortest wavelength CIV points fit well the line derived from the Na- and Li-like calibration. At the longest wavelengths the 384.1Å and 419.6Å points, when combined with the ArXVI 389.1Å and CrXIV 412.0Å points, are consistent with the line, which is close to a straight line in logarithmic space, being extended. Figure 4 also gives error bars to the calibration. It is expected that a  $\pm 10\%$  accuracy is realistic throughout most of the wavelength range, although a  $\pm 15\%$  error bar is given for the lowest wavelength point at 153.5Å, since this is derived by line fitting to the CuXXVII line ratio and no independent confirmation is possible.

Table 6. Coefficients to the polynomial fit to the KT7/2 calibration,  $\lambda > 220\text{Å}$

$a_0$	$a_1$	$a_2$
-0.75608	1.99328e-3	1.36436e-6

c) The sensitivity calibration for weak lines.

Figure 5 illustrates the differences in the line profiles between intense and weak lines, using observations of CIV. Figure 5a shows the intense 384.1Å line observed in pulse 69893, figure

5b the weaker 296.9Å line from pulse 69922, figure 5c the 289.2Å line from pulse 69912 and figure 5d the 244.9Å line from pulse 69932. As discussed in section 2, the sensitivity calibration has been derived for a  $\pm 3$  pixel integration range and it can be seen in figures 5b to 5d that this range is inappropriate for weak lines, for which a  $\pm 2$  pixel integration range should be used. It is therefore necessary to derive the relationship between integrations carried out with a  $\pm 3$  and  $\pm 2$  pixel ranges.

A number of intense lines were used to derive this relationship and these are listed in table 7, together with the mean ratio and the number of pulses used to derive the mean. This analysis produced a wide range of ratios. With so few pixels in a line profile, the ratio is expected to depend on the line profile, but it was also found to depend on the pixel number of the line. This would suggest some variation in the diffraction pattern giving rise to the central region of the line profile at different positions on the detector. Figure 6 shows a plot of the ratio against pixel number, the three curves corresponding to a peaked line profile as illustrated in figure 5b, a flatter profile skewed to the left, 5c, and right, 5d. Polynomial fits were made to the three curves. The pixel number and profile shapes have been added to table 7 and table 8 gives the polynomial fit coefficients.

Table 7. Spectral lines used for the  $\pm 3$  to  $\pm 2$  pixel range integration ratio

Wavelength (Å)	Ion	No. of measurements	Mean ratio and standard deviation	Pixel	Shape of line profile
153.5	Cu XXVII	6	1.42 $\pm$ 0.93%	976	Peaked
165.4	Ni XXVI	5	1.37 $\pm$ 1.09%	933	Flat - skewed right
179.0	Kr XXVI	5	1.51 $\pm$ 0.85%	884	Flat - skewed left
192.0	Fe XXIV	6	1.35 $\pm$ 3.05%	837	Flat - skewed right
206.9	Mn XXIII	1	1.37	784	Peaked
220.1	Kr XXVI	8	1.35 $\pm$ 0.38%	738	Flat - skewed right
223.0	Cr XXII	5	1.50 $\pm$ 1.51%	728	Flat - skewed left
224.8	Cu XXVII	6	1.44 $\pm$ 1.52%	721	Flat - skewed left
234.2	Ni XXVI	7	1.43 $\pm$ 1.52%	689	Flat - skewed right
255.1	Fe XXIV	6	1.53 $\pm$ 2.61%	617	Flat - skewed left
266.9	Mn XXIII	1	1.42	576	Peaked
273.4	Cu XIX	12	1.48 $\pm$ 2.04%	554	Flat - skewed left
279.7	Cr XXII	5	1.59 $\pm$ 2.68%	533	Flat - skewed left
284.2	Fe XV	7	1.48 $\pm$ 1.00%	518	Flat - skewed right
292.0	Ni XVIII	5	1.64 $\pm$ 3.68%	492	Flat - skewed left
312.4	C IV	5	1.41 $\pm$ 0.23%	423	Peaked
320.6	Ni XVIII	5	1.49 $\pm$ 1.96%	396	Peaked
328.3	Cr XIII	6	1.58 $\pm$ 2.76%	371	Flat - skewed left
335.4	Fe XVI	5	1.45 $\pm$ 1.24%	347	Peaked
353.9	Ar XVI	5	1.65 $\pm$ 0.64%	287	Flat - skewed right
360.8	Fe XVI	5	1.53 $\pm$ 1.81%	264	Peaked
384.1	C IV	5	1.72 $\pm$ 0.86%	189	Flat - skewed right
389.1	Ar XVI	5	1.70 $\pm$ 1.03%	173	Flat - skewed right
389.9	Cr XIV	5	1.78 $\pm$ 5.39%	171	Flat - skewed left
412.0	Cr XIV	5	1.66 $\pm$ 5.42%	99	Peaked
419.6	C IV	5	1.79 $\pm$ 1.66%	75	Peaked

It is noted that a criterion was adopted to decide in intermediate cases whether a profile should be classed as 'peaked' or 'flat'. In figure 5b and 5c, if the length AB is greater than the length BC the profile is regarded as peaked and *vice versa*.

Table 8. Coefficients to the polynomial fits to the  $\pm 3$  to  $\pm 2$  pixel range integration ratios

	$a_0$	$a_1$	$a_2$	$a_3$
Peaked	1.82630	-1.30223e-3	9.13310e-7	
Flat - skewed right	1.88281	-6.05069e-4	-3.80942e-7	6.47426e-10
Flat - skewed left	1.90508	-1.13161e-3	5.79114e-7	

## 4. Conclusion

A relative sensitivity calibration for the JET KT7/2 spectrometer has been presented. This has been derived by comparing measured and modelled Na- and Li-like metal line intensity ratios, which together with those of Ar and Kr extend throughout its spectral range. The metals are intrinsic to the plasma, Ar and Kr introduced by gas-puffing. Fewer pulses were found with an intense spectrum of the metal lines than in a corresponding KT2 analysis, this being a particular problem for FeXXIV and CuXXVII. For these ratios, line fitting was used to improve the reliability of the calibration. Despite this a very satisfactory accuracy has been achieved. A similar comparison of measured and modelled CIV line intensity ratios provided confirmation of the calibration derived from the metal line ratios and has allowed the calibration at the longest wavelengths to be improved. The calibration is expected to have an accuracy of  $\sim \pm 10\%$  throughout nearly all of the KT7/2 spectral range. In the VUV spectral region such an accuracy is exceptional and will enhance the use of the spectrometer.

The spectral line profiles on these instruments are unusual in that, although their central regions are similar throughout the spectral range of the instrument, the line wings become submerged in the background as the line becomes weaker. In order to deal with weak lines it is necessary to find the ratio of the  $\pm 3$  to  $\pm 2$  pixel range spectral line integrations for different line profiles and as a function of pixel number. The calibration is determined using intense lines, for which the  $\pm 3$  pixel range integration is used, but a  $\pm 2$  pixel integration range is necessary to give a reliable integration of weak spectral lines.

The presented relative sensitivity calibration is the first step in providing an absolute sensitivity calibration for all three KT7 spectrometers.

This work was carried out within the framework of the European Fusion Development Agreement and was partly funded by the United Kingdom Engineering and Physical Sciences Research Council and by the European Communities under the contract of Association between EURATOM and UKAEA. The views and opinions expressed herein do not necessarily reflect those of the European Commission.

\* See the appendix of F. Romanelli *et al.*, Proceedings of the 22nd IAEA Fusion Energy Conference, 2008, Geneva, Switzerland.

## References

- Aggarwal K M and Keenan F P, 2004, *Phys. Scr.*, **69**, 385  
Fonck R J, Ramsey A T, Yelle R V, 1982, *Appl. Opt.*, **21**, 2115  
Lawson K D *et al.*, 2009a, *JINST* **4** P04013  
Lawson K D *et al.*, 2009b, 'Comparison of modelled C VUV line intensity ratios with observations of the emission from the JET plasma SOL - I', *JET Report*  
Lawson K D *et al.*, 2009c, 'The measurement of JET divertor electron temperatures using VUV spectroscopy', In preparation  
Maggi C F, 1996, Ph.D. Thesis, University of Strathclyde  
Sampson D H, Zhang H L, Fontes C J, 1990, *ADNDT*, **44**, 209  
Schwob J L, Wouters A W, Suckewer S, Finkenthal M, 1987, *Rev. Sci. Instrum.*, **58**, 1601  
Summers H P, 2004, 'The ADAS User Manual, version 2.6', <http://adas.phys.strath.ac.uk>  
Whiteford A D, Badnell N R, Balance C P, Loch S D, O'Mullane M G, Summers H P, 2002, *J. Phys. B*, **35**, 3729  
Wolf R C *et al.*, JET Preprint, JET-P(95)34  
Zacks J, 2009, Ph.D. Thesis, Queen's University, Belfast  
Zhang H L, Sampson D H, Fontes C J, 1990, *ADNDT*, **44**, 31

## Figure captions

- Figure 1. The KT7/2 spectrum for JET pulse 67966 averaged between times 9.3 and 9.4s.  
Figure 2. The Na- (+) and Li-like (\*) inverse sensitivity ratios plotted against wavelength for - Ar, - Cr, - Mn, - Fe, - Ni, - Cu, - Kr.  
Figure 3. The KT7/2 spectrum for JET pulse 69931 averaged between times 2.3 and 2.6s.  
Figure 4. The relative inverse sensitivity calibration ( $S^{-1}$  at  $312.4\text{\AA} = 1$ ) for KT7/2. + points derived from the Na- and Li-like ratios, \* from CIV ratios. — 2nd order polynomial fit.  
Figure 5. Spectral line profiles of the CIV a)  $384.1\text{\AA}$  line, pulse 69893 (13.5-16.0s), b)  $296.9\text{\AA}$  line, pulse 69922 (2.0-3.0s), c)  $289.2\text{\AA}$  line, pulse 69912 (22.0-28.0s) and d)  $244.9\text{\AA}$  line, pulse 69932 (13.5-19.5s).  
Figure 6. Ratio of integrations using  $\pm 3$  and  $\pm 2$  pixel ranges, with + peaked profile,  $\diamond$  flat profile skewed right and \* flat profile skewed left.

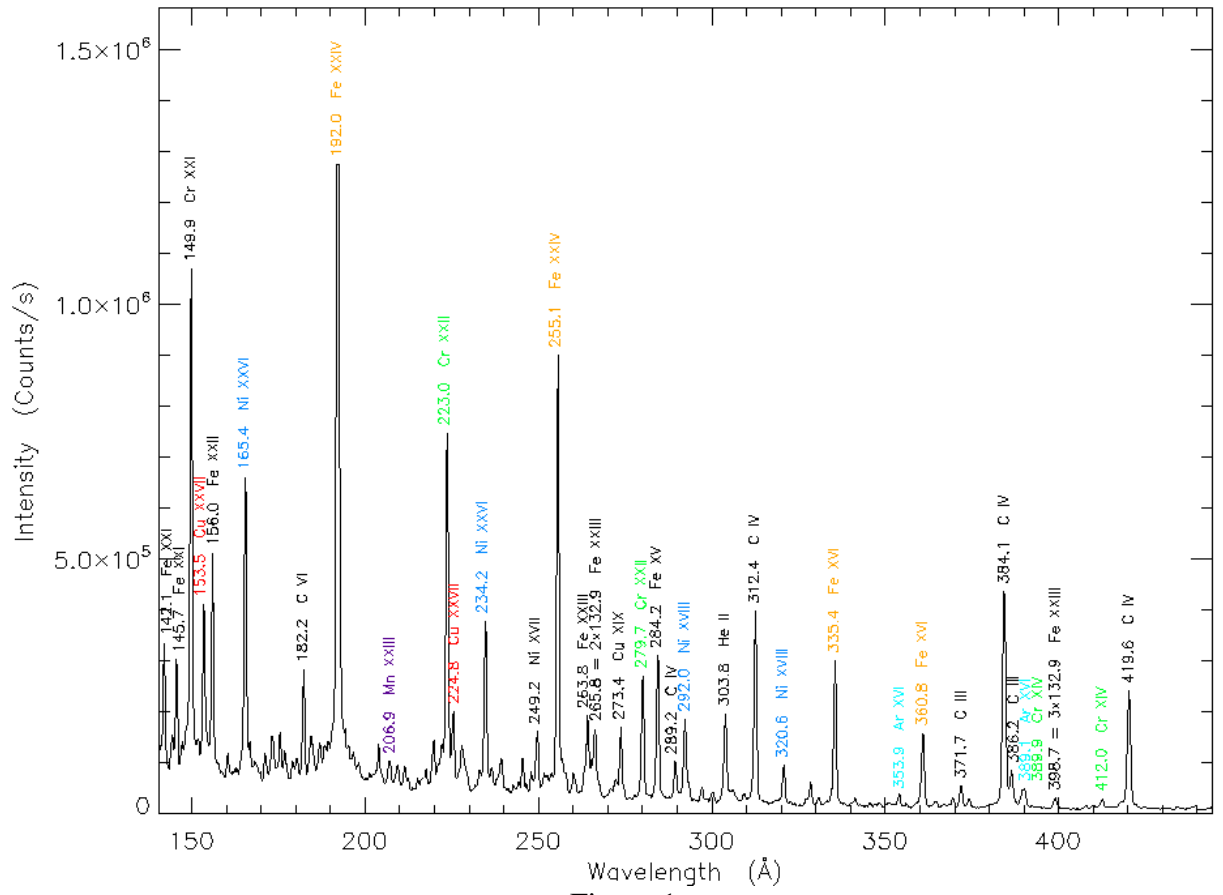


Figure 1.

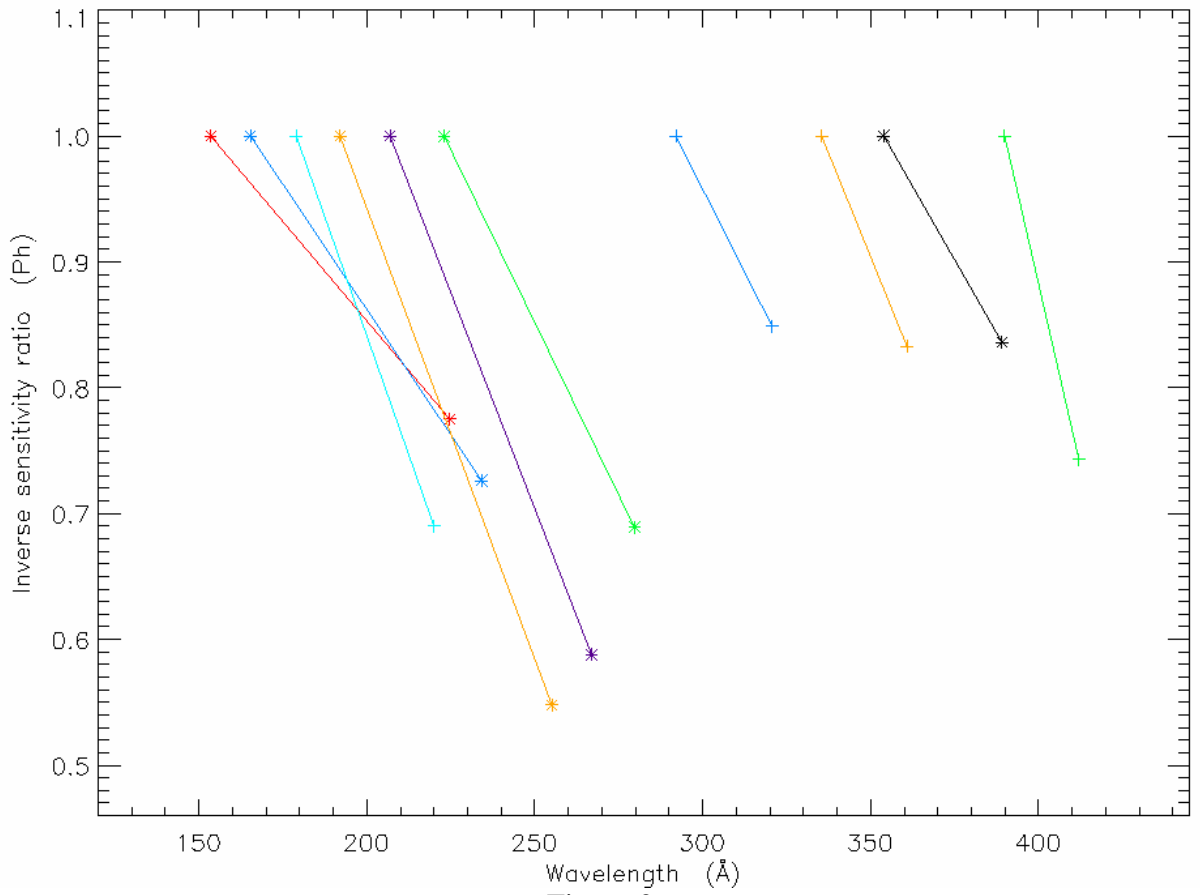


Figure 2.

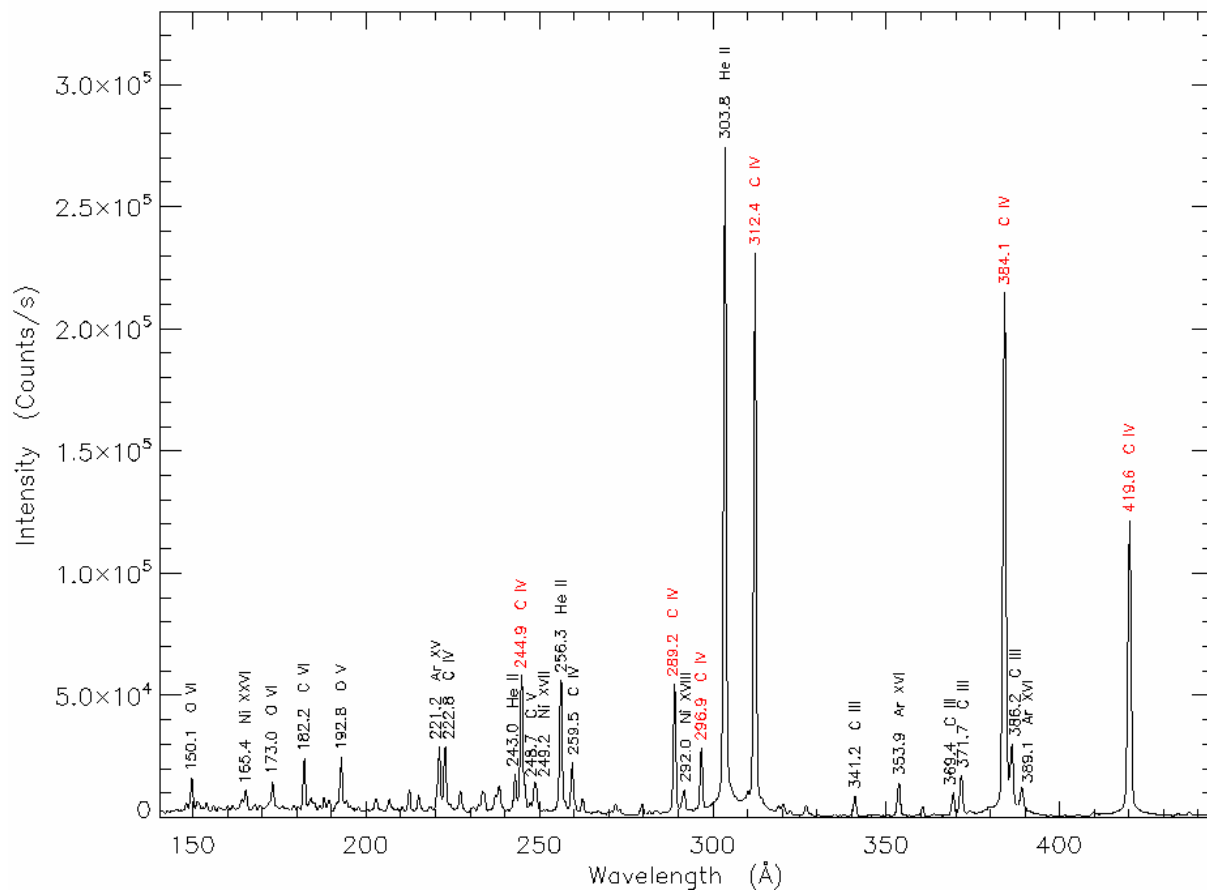


Figure 3.

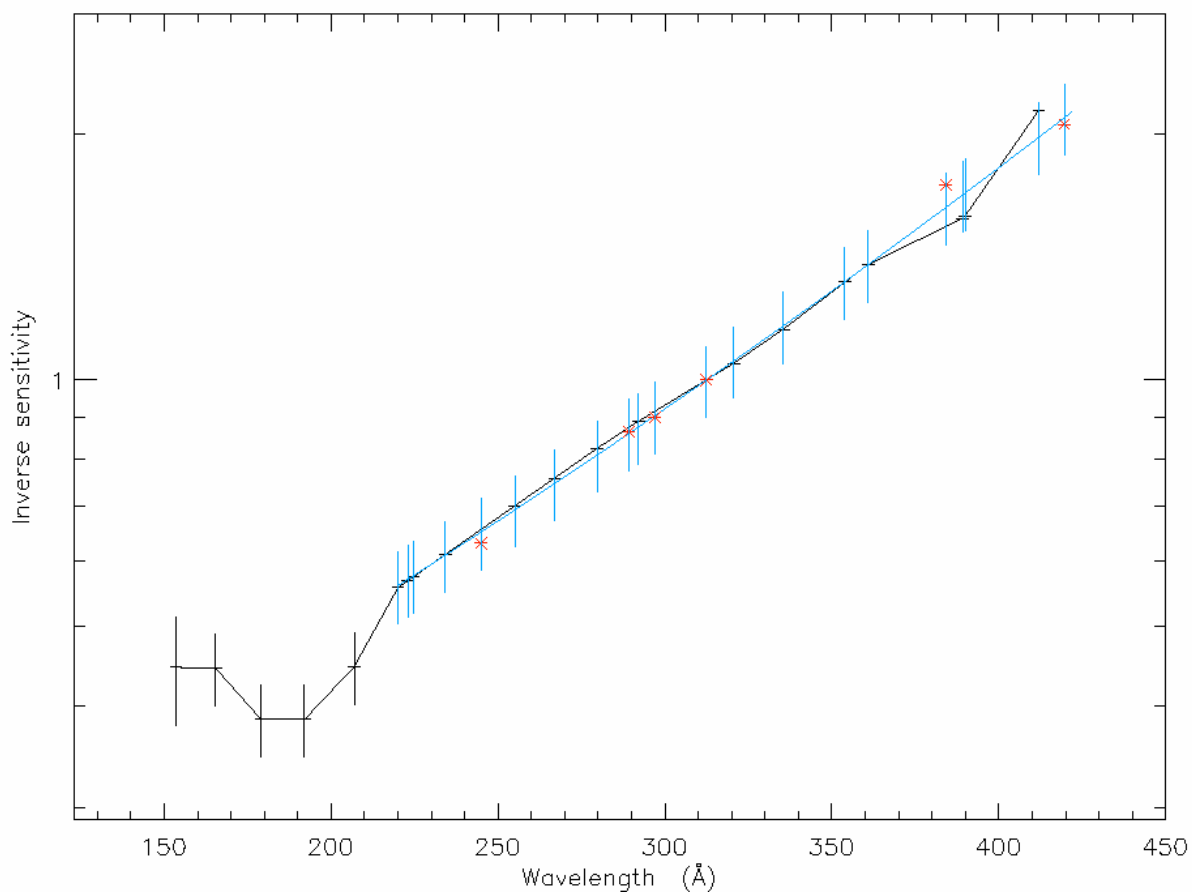


Figure 4.

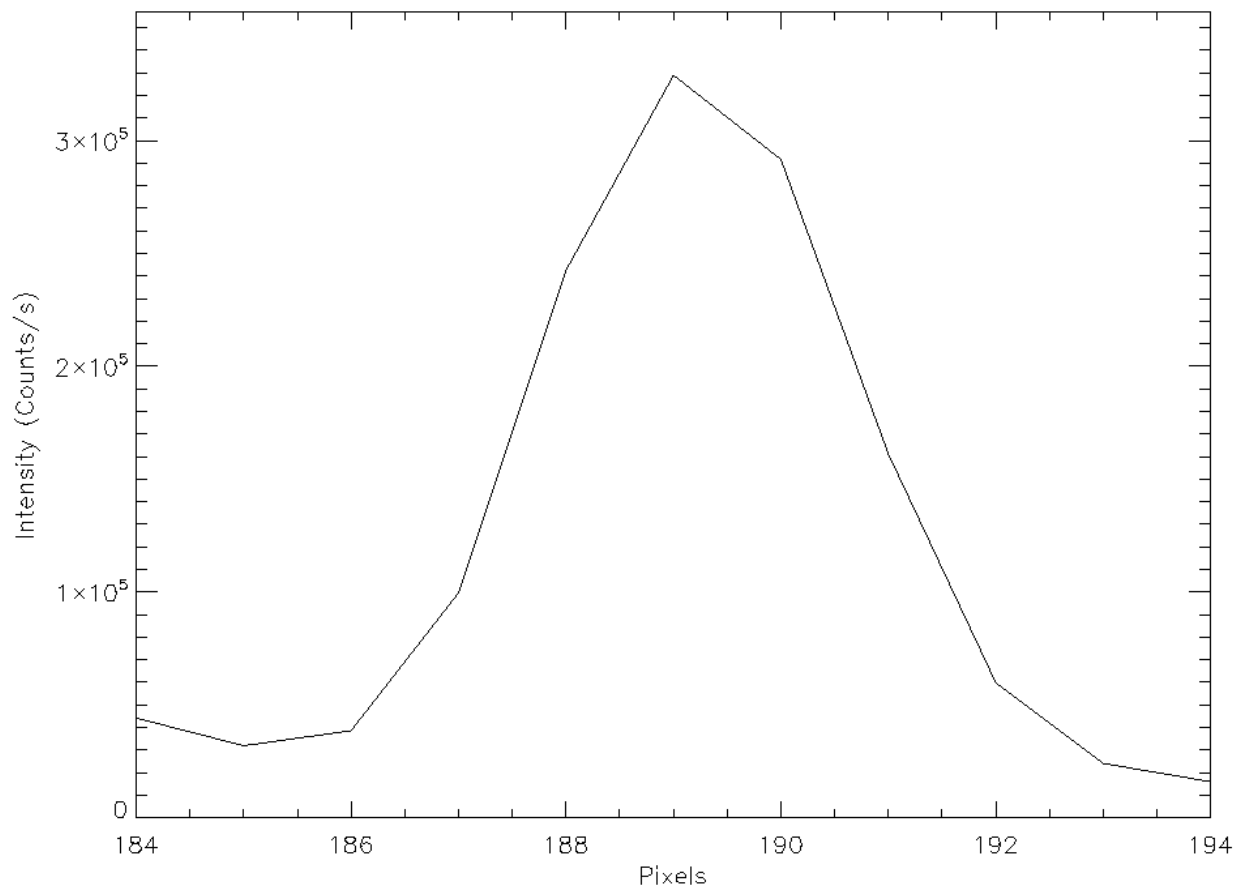


Figure 5a.

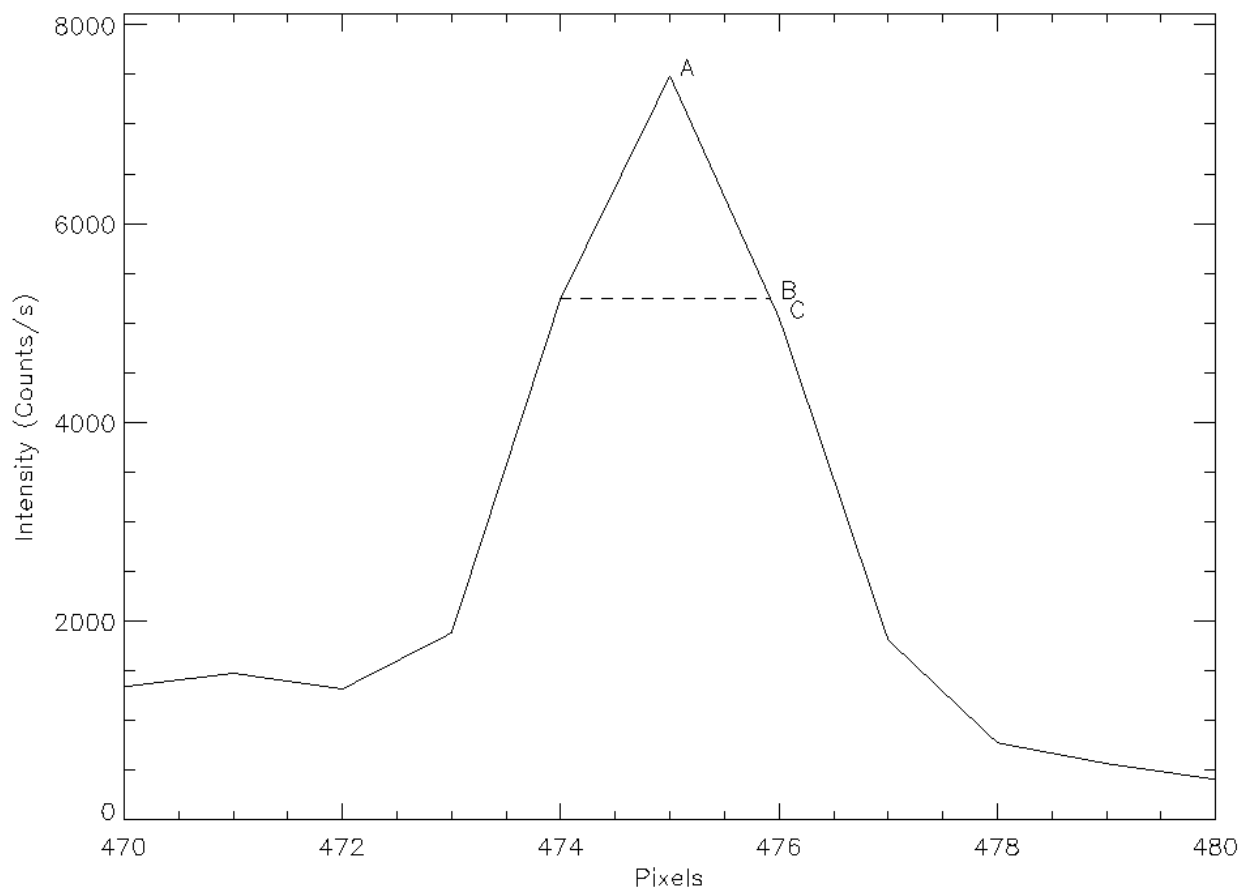


Figure 5b.



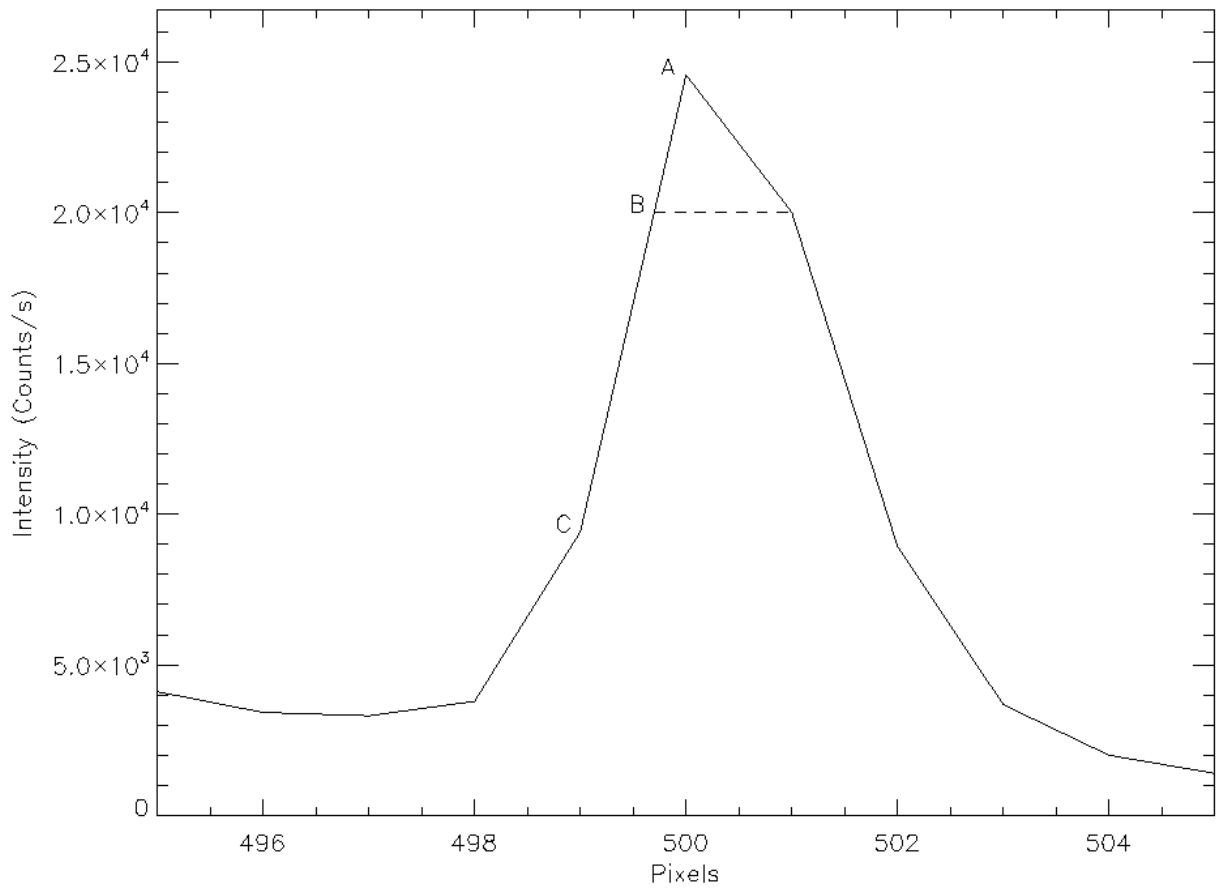


Figure 5c.

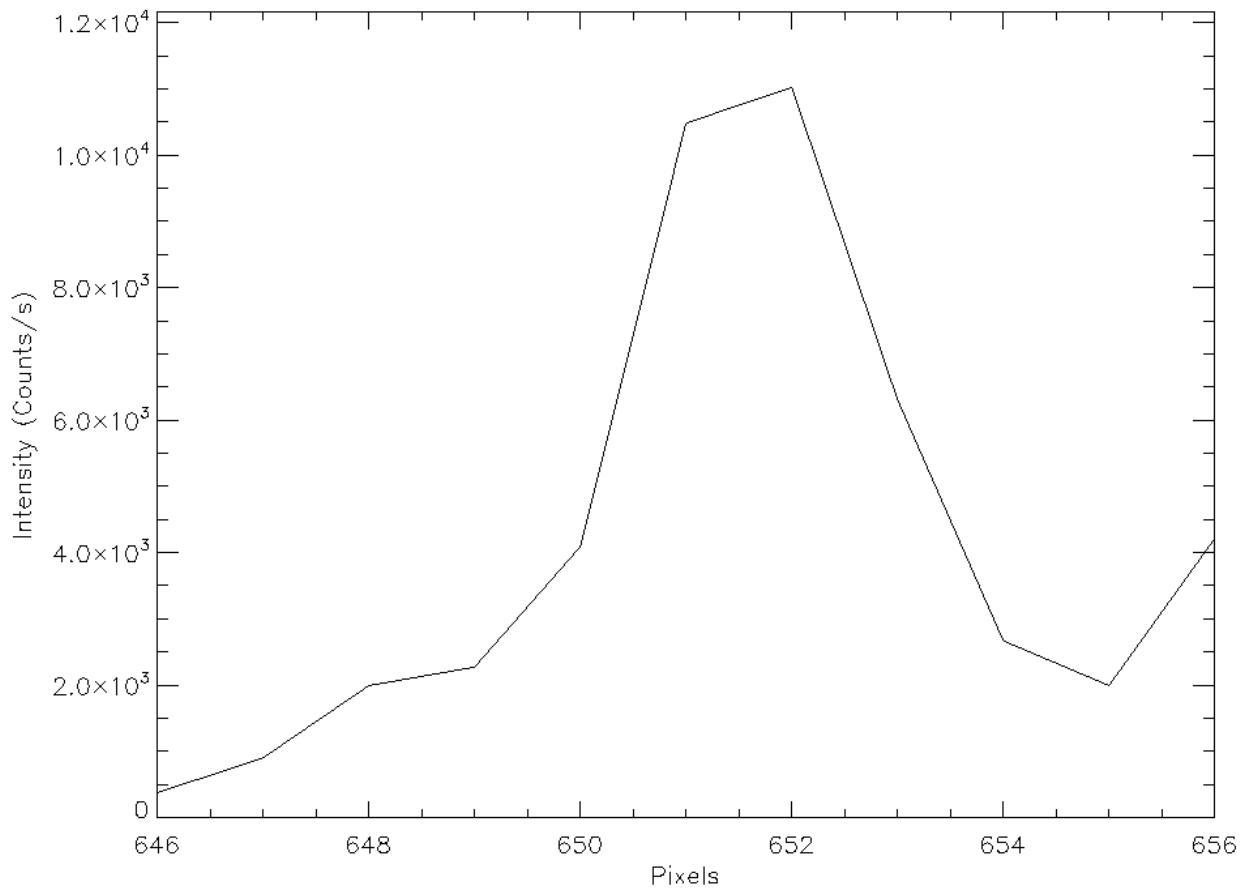


Figure 5d.

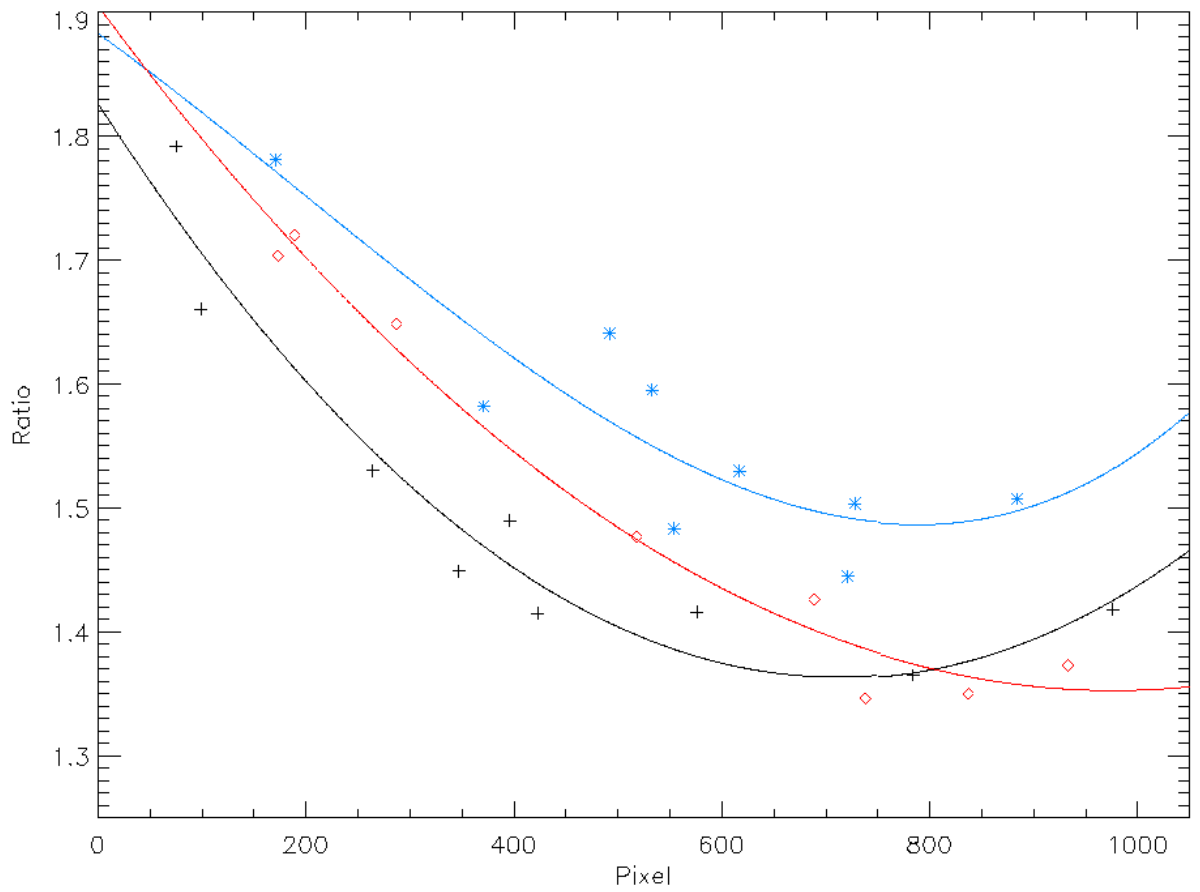


Figure 6.